JGR Space Physics

RESEARCH ARTICLE
10.1029/2018JA026327

Electron Density Profiles in the Upper Ionosphere of Mars From 11 Years of MARSIS Data: Variability Due to Seasons, Solar Cycle, and Crustal Magnetic Fields

F. Duru[1,2], B. Brain[1], D. A. Gurnett[2], J. Halekas[2], D. D. Morgan[2], and C. J. Wilkinson[3]

[1]Department of Physics, Coe College, Cedar Rapids, IA, USA, [2]Department of Physics and Astronomy, University of Iowa, Iowa City, IA, USA, [3]Department of Materials Sciences and Engineering, Pennsylvania State University, University Park, PA, USA

Key Points:
- Electron density increases with decreasing altitude with an *e*-folding height changing between 45 and 120 km from 0 to 120 degrees of SZA
- Data for a full solar cycle show that the average electron density values are directly related to the solar activity
- Electron densities are higher during northern winters and above strong crustal magnetic fields on the dayside

Correspondence to:
F. Duru,
firdevs-duru@uiowa.edu

Citation:
Duru, F., Brain, B., Gurnett, D. A., Halekas, J., Morgan, D. D., & Wilkinson, C. J. (2019). Electron density profiles in the upper ionosphere of Mars from 11 years of MARSIS data: Variability due to seasons, solar cycle, and crustal magnetic fields. *Journal of Geophysical Research: Space Physics*, *124*, 3057–3066. https://doi.org/10.1029/2018JA026327

Received 20 NOV 2018
Accepted 24 FEB 2019
Accepted article online 07 MAR 2019
Published online 23 APR 2019

Abstract The Mars Advanced Radar for Subsurface and Ionosphere Sounding on board the Mars Express spacecraft measures the frequency of local plasma oscillations, which can be used to determine electron densities local to the spacecraft. This paper provides an overview of electron densities in the upper Martian ionosphere, obtained by investigating over 400,000 ionograms, during the course of about 11 years, corresponding to a full solar cycle. The data cover wide latitude and longitude ranges, 180° of solar zenith angle (SZA), and altitudes from about 250 to 1,550 km. The electron density profiles show large fluctuations within each orbit and also for any given altitude and SZA range. However, the median electron density is almost constant on the dayside at a fixed altitude range, with the exception of a dip at around 30° SZA, at altitudes between 300 and 600 km. A sudden drop in density is observed as the terminator is approached from the dayside. For a fixed SZA range, the median electron density decreases exponentially with increasing altitude. The high-altitude scale height is composed of two exponential functions of SZA joined near the ionospheric terminator. The *e*-folding height changes between 45 and 214 km from the subsolar point up to 120°, corresponding to effective temperatures between about 165 and 780 K. Solar activity has a clear effect on the median electron densities above 500 km and on *e*-folding height. The median electron density is higher during northern winters, as well as above regions of strong crustal fields on the dayside.

1. Introduction

The Mars Express (MEX) spacecraft, which is in an eccentric orbit around Mars, has been providing valuable data since 2005 (Chicarro et al., 2004). The low-frequency radar MARSIS (Mars Advanced Radar for Subsurface and Ionosphere Sounding) is one of the six instruments on board MEX (Picardi et al., 2004). MARSIS provides electron densities in the ionosphere through radar sounding, as well as local electron densities through the excitation of electron plasma oscillations (Gurnett et al., 2005). In this study, we give an overview of the electron densities of the upper ionosphere of Mars (altitudes between ~250 and 1,550 km) with 11 years of local plasma density from plasma oscillations. This work presents the seasonal, solar cycle, and crustal field effects on the electron densities in the upper ionosphere of Mars. It also extends the study provided by Duru et al. (2008), which was performed with 2 years of MARSIS data.

The ionosphere of Mars has been studied with different techniques. Radio occultation measurements, which utilize the phase shift of a radio signal that propagates through the ionosphere to determine the column electron density (Schunk & Nagy, 2009), provide information about the ionospheric density and structure. Studies by Kliore et al. (1965), Fjeldbo et al. (1966), Zhang et al. (1990), Patzold et al. (2005), and others utilize this method. The first direct ion measurements in the Martian ionosphere came with analyzers on Viking 1 and 2 (Hanson et al., 1977). Since 2015, The Mars Atmosphere and Volatile EvolutioN (MAVEN) mission (Jakosky et al., 2015) has been providing valuable information about the plasma environment of Mars. Ergun et al. (2015) provided first in situ electron temperature profiles, along with electron densities measured with Langmuir Probe and Waves instrument on MAVEN. Nightside density and temperature measurements from Langmuir Probe and Waves are reported by Fowler et al. (2015).

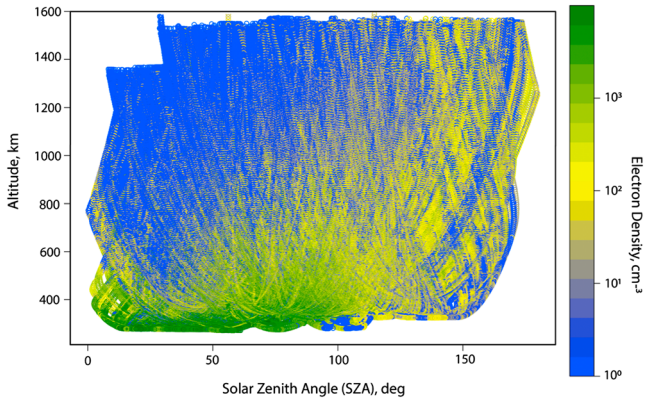

Figure 1. Altitude and SZA coverage of the data with color bars representing the electron density.

2. Data

In this study, we use local electron densities obtained from plasma oscillation harmonics (Duru et al., 2008). In ionospheric sounding mode, the MARSIS transmitter excites electrostatic oscillations at the local plasma frequency surrounding the spacecraft. Due to the high intensity of the electron plasma oscillations, the received waveforms are often severely clipped introducing harmonics at multiples of fundamental plasma frequency. The spacing between the harmonics then provides the local electron plasma frequency, even when the fundamental frequency is lower than the lower limit of the frequency, 100 kHz. Once the electron plasma frequency, f_p, is obtained the corresponding local electron density is found by using $f_p = 8{,}980\sqrt{ne}$, where f_p is in hertz and n_e is in per cubic centimeter (Duru et al., 2008; see, e.g., Gurnett & Bhattacharjee, 2005).

This study uses data obtained between September 2005 and June 2016, corresponding to about six Martian years, about one solar cycle. The altitude and solar zenith angle (SZA) coverage with color-coded electron density values is provided in Figure 1. The altitude range is between ~250 and 1,550 km. For the present study, local electron density data are available over the full range of SZA, from 0° to 180°. The nightside ionosphere of Mars has been studied by Duru et al. (2011) using local electron densities; however, the data were only available at SZA less than 150°. Beyond ~160°, data are available only at altitudes higher than 800 km. The SZA coverage changes with time: Coverage at low SZA is less frequent later in the mission.

In this study, more than 1,300 orbits have been studied. The electron density for each pass is plotted as a function of universal time. Every orbit shows the expected trend: the electron density is low at high altitudes and increases as the spacecraft approaches periapsis. As the spacecraft ascends, the electron densities decrease. The electron density fluctuates during each orbit, with timescales ranging from a few seconds to minutes (Gurnett et al., 2005, 2010). Fluctuations indicate electron density changes of more than 1 order of magnitude in a few seconds in about 40% of the passes. The density profile is smoother in 60%. Electron densities show orbit-to-orbit variations, too. Orbit-to-orbit and within-orbit variations in the neutral densities and temperatures, as well as in the ionosphere, are noted by Bougher, Jakosky, et al. (2015) in MAVEN data, as well.

It should also be noted that when the spacecraft is in the solar wind instead of the ionosphere the harmonics of electron plasma oscillations are not observed (Duru et al., 2008; Duru et al., 2010). As a consequence, in many passes the electron plasma oscillations are not observed at high altitudes and this altitude, which marks the boundary between the ionosphere and solar wind, is SZA dependent.

3. Electron Density Profiles as a Function of SZA

The behavior of the electron density with changing SZA is examined with a series of plots in Figure 2, where electron density is plotted as a function of SZA. As stated, the electron plasma oscillations are not observed when the spacecraft is in the solar wind. So the density value is recorded as 0 for those regions. This does not necessarily mean that the density is 0; it means that it is undetectable. To correct for this bias, instead of using averages, we plotted the median values including zeros, as a function of SZA for a series of fixed altitude ranges, as shown in Figure 2. In this figure, a series of such plots for the altitude ranges between 200 and 300, between 300 and 400, and between 1,100 and 1,200 km are shown. The results mostly confirm Duru et al. (2008) and are also consistent with simulations provided in the same paper. At low altitudes, as seen in Figure 2a, the median electron density is almost constant on the dayside. Due to the fluctuating nature of data, it shows small variations. Around the terminator, the electron density decreases abruptly. The median density is ~4,000 cm^{-3} up to ~75° between 200 and 300 km and drops to ~200 cm^{-3} at around 110°.

As the altitude increases, the median electron density decreases. However, constant density on the dayside with sudden decrease around the terminator can still be observed up to about 800 km. From

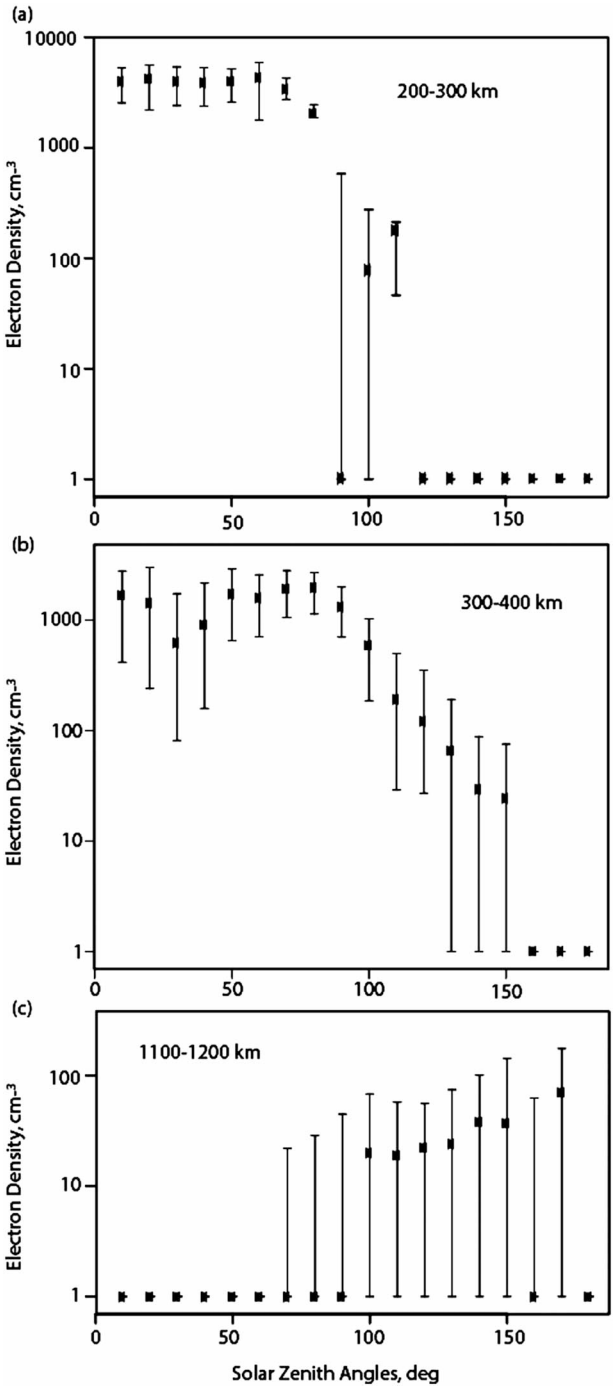

Figure 2. Median electron density as a function of solar zenith angle for three different altitude ranges: (a) 200–300 km, (b) 300–400 km, and (c) 1,100–1,200 km. Error bars show upper and lower quartiles for a given solar zenith angle range.

~800 km, the electron densities on the dayside become so low that the difference with the nightside becomes very small. In Figure 2c, for example, the median density in the altitude range between 1,100 and 1,200 km is almost always less than 100 cm^{-3}. A small increase is observed for SZAs above 150°. At low SZAs the shocked solar wind boundary penetrates deeper, leading to zero density medians at high altitudes, as seen in Figure 2c. Figure 2 also provides the upper and lower quartiles (25th and 75th quartiles) to show the extent of fluctuations for a given SZA value. The upper and lower quartiles are very different, in some cases having more than 1 order of magnitude between them, implying large fluctuations.

A dip in the density at around 25° SZA is observed at altitudes between 300 and 500 km. A similar trend could be seen in the data shown in Figure 9 of Duru et al. (2008), albeit with lower amplitude. It should be noted that the dip is inside the error bars of that SZA range, but it is only observed at this altitude and SZA range. A similar dip, this time in temperatures of Ar, CO_2, and O at altitudes between 200 and 300 km was also seen in Mahaffy et al. (2015).

4. Electron Density Profiles as a Function of Altitude

To obtain a better understanding of the behavior of the electron densities in the upper Martian ionosphere, we investigate electron density versus altitude for fixed SZA ranges. Figure 3 presents the median electron density as a function of altitude for six 30° SZA ranges, where the median is calculated for every 15-km altitude bin. The median density decreases with increasing altitude up to 120°. The density is low on the deep nightside and does not vary significantly with altitude. At high altitudes above the dayside and flanks, an increase is observed in the density. This increase is dependent on the SZA range (above 500 km for 0–30°, around 1,500 km for 30–120°). For SZAs between 30° and 60°, an increased density is still present at altitudes higher than 1,500 km. This region includes elevated electron density values from May 2012, during which some solar flares were observed.

Again, to correct for this bias and to have another point of view to the data, we plotted the median values including the data points where no plasma harmonics were detected. As the SZA increases, the height of the shocked solar wind boundary increases, leading to more nonzero data at high altitudes for high SZAs. In Figure 4 the median value is given by the blue dots. At altitudes above 500 km the median electron density is 0 for the 0° to 30° SZA range. Figure 4 also includes the lower (green points) and upper quartiles (red points). Again, the fluctuations at a given altitude result in a difference of more than 1 order of magnitude in many SZA and altitudes.

5. The High-Altitude Plasma-Scale Height

The median values of the density on Figure 4 can be used to estimate the plasma-scale height. We have done exponential fits on the segment of the median values to obtain the function of high-altitude plasma-scale height as a function of SZA. The 25th and 75th percentiles were used to estimate upper and lower values of the scale height with the average of these values taken as an uncertainty on the measurement. Figure 5 gives the results of this analysis. We see that the scale height as a function of SZA is well described as an exponential function given by

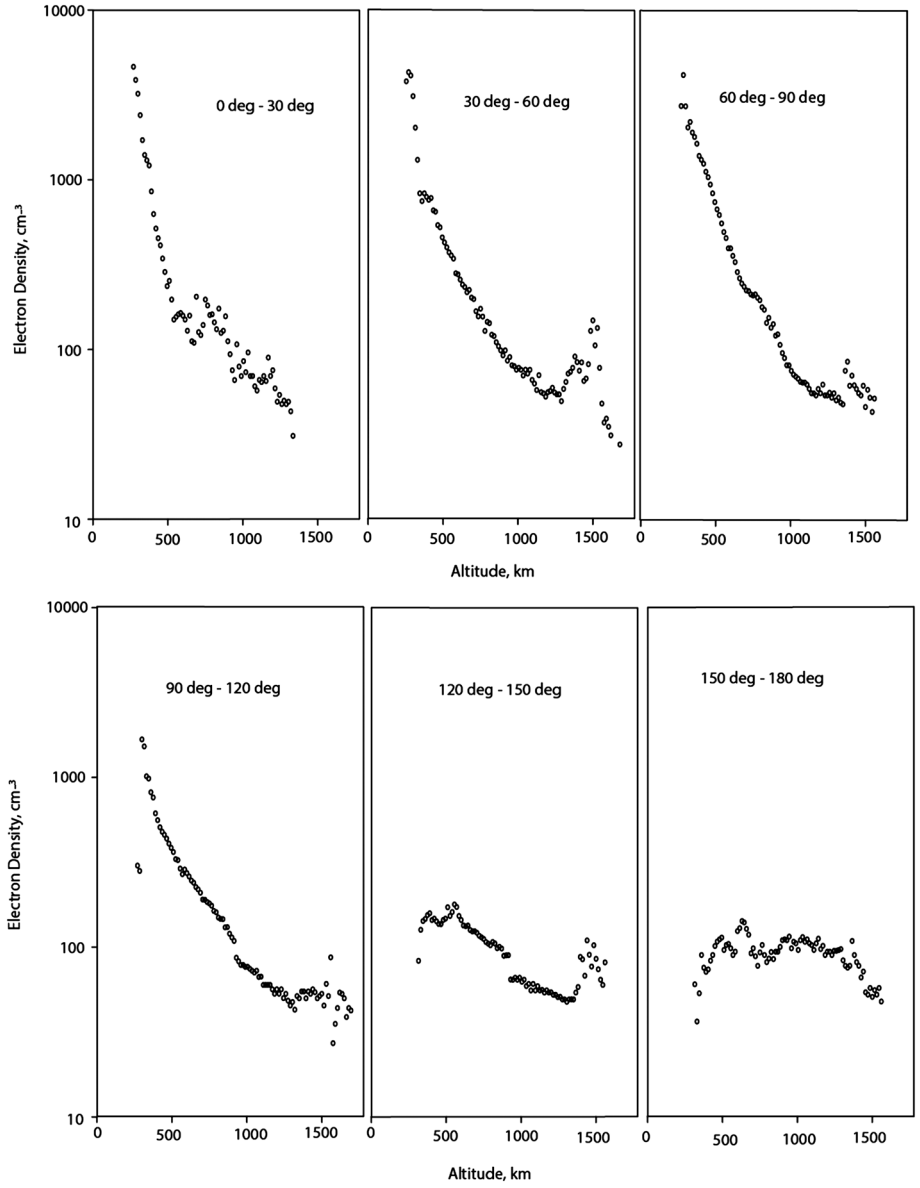

Figure 3. Median electron density, in logarithmic scale, as a function of altitude for six different solar zenith angle ranges.

$$\log_{10}\left(\mathrm{H_p}\,[\mathrm{km}]\right) = 1.516 + 0.007611\times\mathrm{SZA}\,(^{\circ}).$$

Note that for the ionosphere, the effective terminator is usually assumed to be 107°. We chose to present data up to 105° since the nightside region is dominated by impact ionization and/or transport from the dayside.

The *e*-folding height changes between about 45 km (at SZA between 0° and 30°) and 214 km (between 90 and 120 km). Assuming the plasma-scale height is given by the *e*-folding height, we calculate the corresponding effective temperatures using $H_p = 2kT/mg$ (Schunk & Nagy, 2009). Assuming that O^+ is the main ion species at the altitudes of our interest and neglecting the gravity variations with the altitude, the effective plasma temperatures in the ionosphere are calculated to be between about 165 and 780 K between subsolar point and 120°.

6. Solar Cycle Dependence of Electron Densities

The Sun's activity shows a cyclic behavior, with a period of 11 years. In this period the sunspots, solar radiation, and appearance of the Sun change. In particular, variations in the intensity of ionizing solar

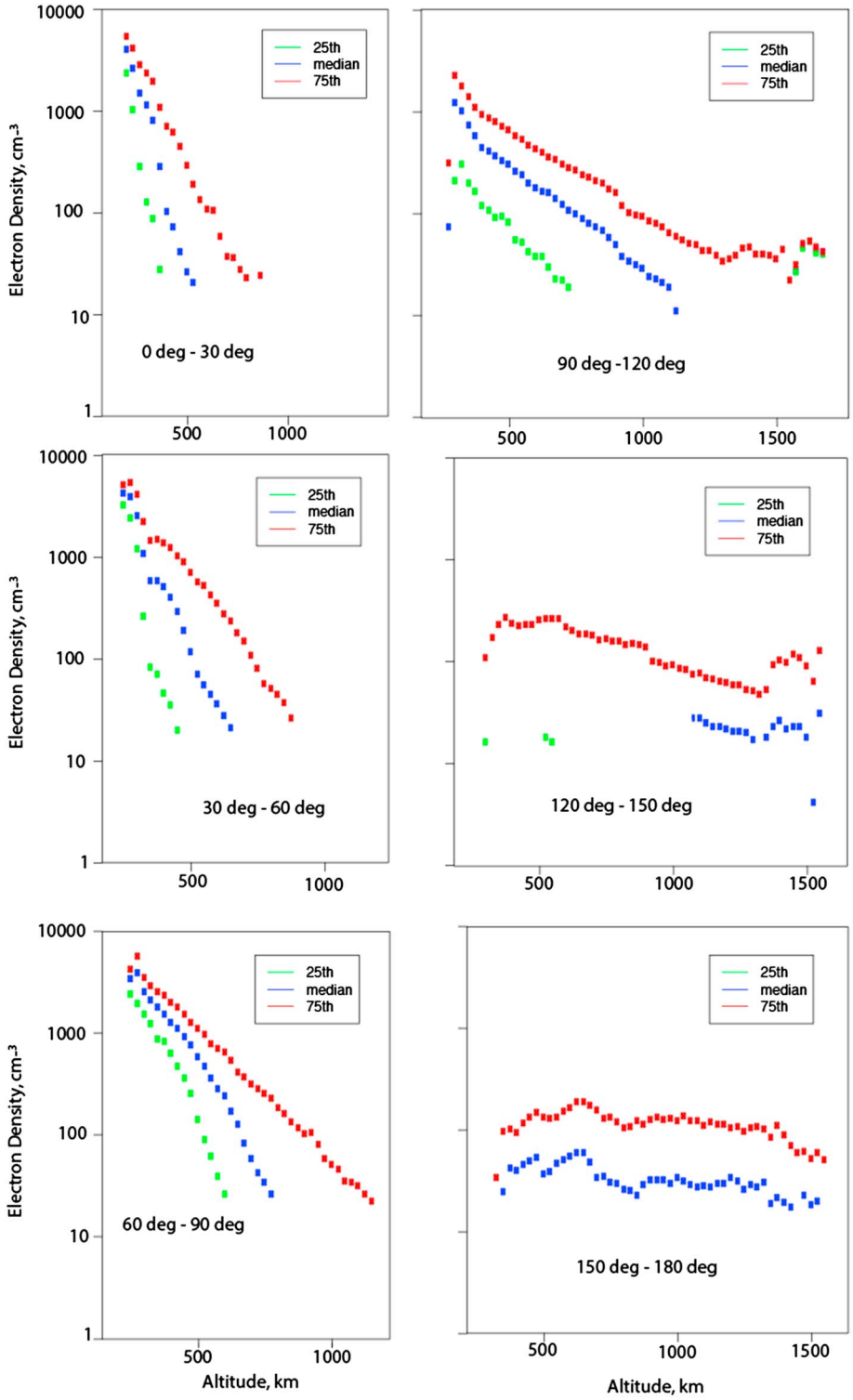

Figure 4. Median electron density (blue dots) as a function of altitude. The 25th and 75th percentiles are shown by the green and red dots, respectively.

flux during a solar cycle result in density variations in the ionospheres of the planets. There have been studies on the density changes in the Martian ionosphere. However, most of these studies considered only a partial solar cycle (Morgan et al., 2008; Fox and Yeager, 2009; Withers and Mendillo, 2005).

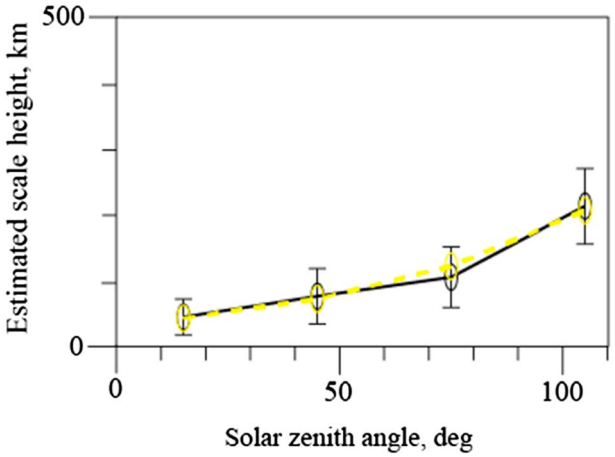

Figure 5. Linear model of the high-altitude scale height based on slopes from Figure 4, along with the error bars.

Recently, Withers et al. (2014) studied the variations in the peak electron densities in the ionosphere of Mars over a full solar cycle, using the combined data from two spacecraft, Mars Global Surveyor and MEX, concluding that the ionospheric peak electron density increases smoothly as the $F_{10.7}$ value increases up to 130 units. However, the data were very scattered. Lundin et al. (2013) showed that the average ion escape rate increases by a factor of 10 from solar minimum to solar maximum. Bougher, Pawlowski, et al. (2015) used a Mars Global Ionosphere-Thermosphere Model (M-GITM) and showed that the solar cycle and solar rotation timescales have significant effects on the composition, temperature, and global wind structure in the upper atmosphere of Mars. Sanchez-Cano et al. (2016) concluded the solar cycle has a clear effect on the neutral scale height, which is an important parameter in describing the density distribution in the ionosphere.

In this paper, we provide observations on the electron density variations in the upper ionosphere for over 11 years of data, which corresponds to about one full solar cycle. Our data start in 2005, toward the end of solar cycle 23 (see the Space Weather Prediction Center webpage). The current solar cycle, solar cycle 24, began with a minimum on January 2008 and continued with minimum activity until early 2010. It showed two maximums: in 2011 and in 2015, after which the solar activity is slowly decreasing (see http://www.swpc.noaa.gov).

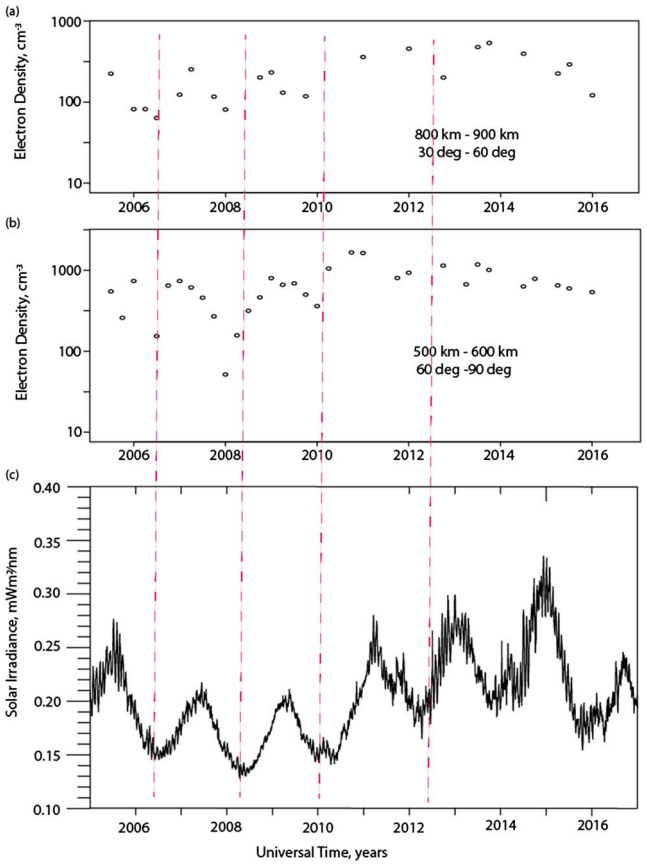

Figure 6. (a) Median electron density as a function of time for the altitude range 800–900 km and SZA range between 30° and 60°. (b) Median electron density as a function of time for the altitude range 800–900 km and SZA range between 30° and 60°. (c) Solar irradiance at 30.5 nm from Thermosphere, Ionosphere, Mesosphere Energetics and Dynamics—Solar EUV Experiment scaled to Mars' distance.

For specific SZA and altitude ranges, we plotted median electron density as a function of time. Figures 6a and 6b are plots for the ranges of 800–900 km and 30–60° and 500–600 km and 60–90°, respectively. The median electron density shows a slight increase during the solar maximum times. However, there are almost periodic dips and peaks in the data, which appear to be correlated with EUV solar irradiance at a wavelength of 30.5 nm from the Thermosphere, Ionosphere, Mesosphere Energetics and Dynamics—Solar EUV Experiment scaled to Mars distance (Figure 6c). The variations in solar irradiance with an approximate 2-year period, seen in Figure 6c, are due to the annual variation in Mars distance from the Sun. Because of the changing distance of Mars, the data in panel c there are five main peaks, which are periodic, with maximums at mid-2005, mid-2007, mid-2009, mid-2011, and mid-2013, and five periodic dips with minimums at mid-2006, mid-2008, mid-2010, and mid-2012. Even with these fluctuations, it is possible to notice the slightly increasing trend of the solar irradiance moving from solar minimum to solar maximum. These dips and peaks correspond to or are followed by the ones observed in MARSIS data.

As seen in the coverage plot, Figure 1b, the data coverage is not homogeneous throughout the time. We mostly focused on the altitude and SZA ranges where we have data for all 11 years. Since the main driver for the electron density on the dayside is photoionization, the solar cycle is expected to affect the dayside densities. Even though expected otherwise, the effect is less obvious at altitudes lower than 500 km. Previous studies showed that precipitating electrons are important factors in sustaining the nightside ionosphere, as well as day to night plasma transport (Fowler et al., 2015; Girazian et al., 2017; Zhang et al., 1990). A similar but diminished trend, not shown here due to insufficient data, has been observed on the nightside.

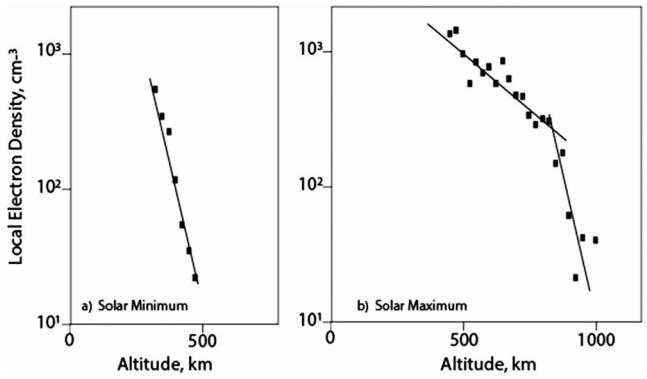

Figure 7. Median electron density (blue dots) as a function of altitude for restricted local time, between 13 and 17 hr for (a) one Martian year around solar minimum and (b) one Martian year around solar maximum. The solid lines indicate rough fits to the data.

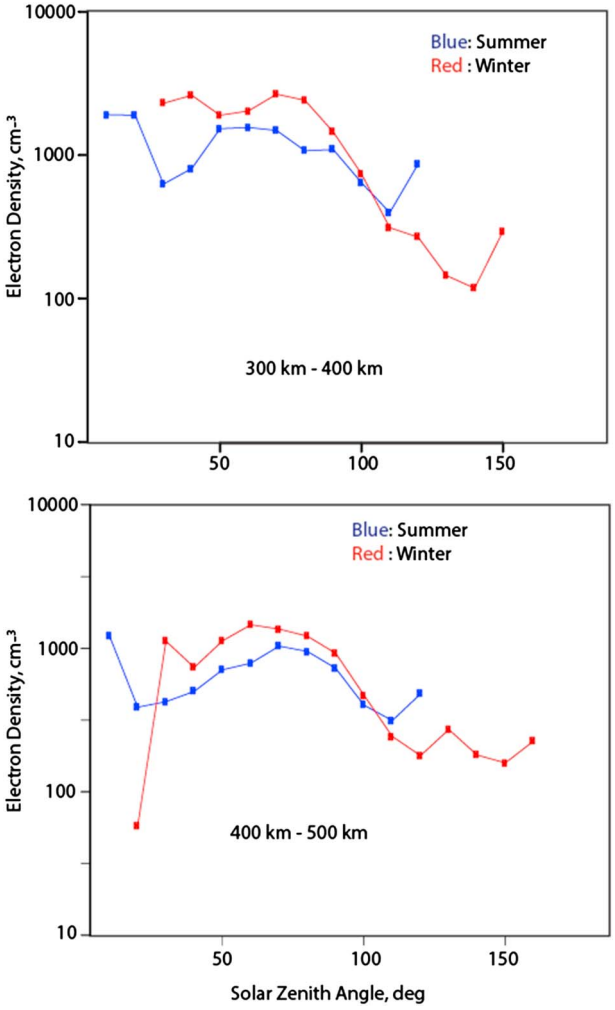

Figure 8. Median electron density as a function of SZA for northern summer (blue dots) and northern winter (red dots) for the altitude range between 300 and 400 km (a) and between 400 and 500 km (b). To exclude the effects of crustal magnetic fields, the data from the region of strong crustal fields (latitudes below 0° and longitude between 150° and 240°).

7. Scale Height as a Function of Solar Cycle

It is interesting to use our abundance of plasma density data to gauge the effect of solar cycle on plasma-scale height. To do this, we have sampled the electron density for one Mars year (687 Earth days) starting 2008, around solar minimum, and starting 2013, around solar maximum. For these two samples we have restricted the SZA to the range 30–60° and the local time to the range 13–17 hr. The results are shown in Figure 7 (part a for solar minimum and part b for solar maximum). Around solar minimum we find a single consistent scale height of 47.7 km, corresponding to an effective temperature of about 175 K. Around solar maximum we find a distinct boundary, at approximately 800 km, between two physical regimes. This dual-scale height regime implies that near solar maximum there is a temperature boundary at around 800 km, corresponding to the approximate altitude of the magnetic pileup boundary at these SZAs (Vignes et al., 2000). The ionospheric plasma-scale height is computed to be 244.7 km, corresponding to about 895 K.

8. Seasonal Dependence of the Electron Densities

Mars experiences all four seasons with more variations than on Earth. The seasons on Mars are strongly affected by the distance from the Sun to Mars. Northern summers are cooler and northern winters are milder due to the eccentricity of the orbit. The seasons in the southern hemisphere are more extreme. Seasons affect the temperatures, exobase height, electron density, O density, and ion peak density in the ionosphere (Valeille et al., 2009). Yamauchi et al. (2015) show that the occurrence rate of pickup ions increases during orbital summer, around Mars perihelion. More recently, observations of Solar Wind Ion Analyzer on board the MAVEN spacecraft by Halekas et al. (2017) confirm strong seasonal variation of the hydrogen corona. According to Rahmati et al. (2018), the MAVEN data show that the H escape rates are about 1 order of magnitude higher near perihelion than that of aphelion.

Figure 8 shows the median density as a function of SZA for different seasons for the northern and southern hemispheres combined. However, to minimize any effect due to crustal fields, we excluded the southern hemisphere longitudes between 150° and 240°. The blue data are for solar longitudes between 0° and 180° corresponding to northern spring and summer, and red is for longitudes between 180° and 360° corresponding to autumn and winter in the northern hemisphere. The southern hemisphere data are also included in the plots by reversing the seasons. The top panel is for the altitude range between 300 and 400 km, and the bottom one is for between 400 and 500 km. As can be seen from the plots, the median electron densities are higher for the winter for most of the dayside. This is consistent with the findings of Morgan et al. (2008) who showed that the average subsolar peak electron density is higher near the southern summer solstice, about 1.8×10^5 cm^{-3} and lower near the northern summer solstice, about 1.4×10^5 cm^{-3}. This trend continues only a couple hundred kilometers. After about 500 km the relationship is not observed anymore. Even though the data on the nightside is scarce, we can say that the same trend is not true for the nightside. It is worth noting that even when the strong crustal field regions are not excluded, the behavior of the median density as a function of seasons is very similar but less pronounced.

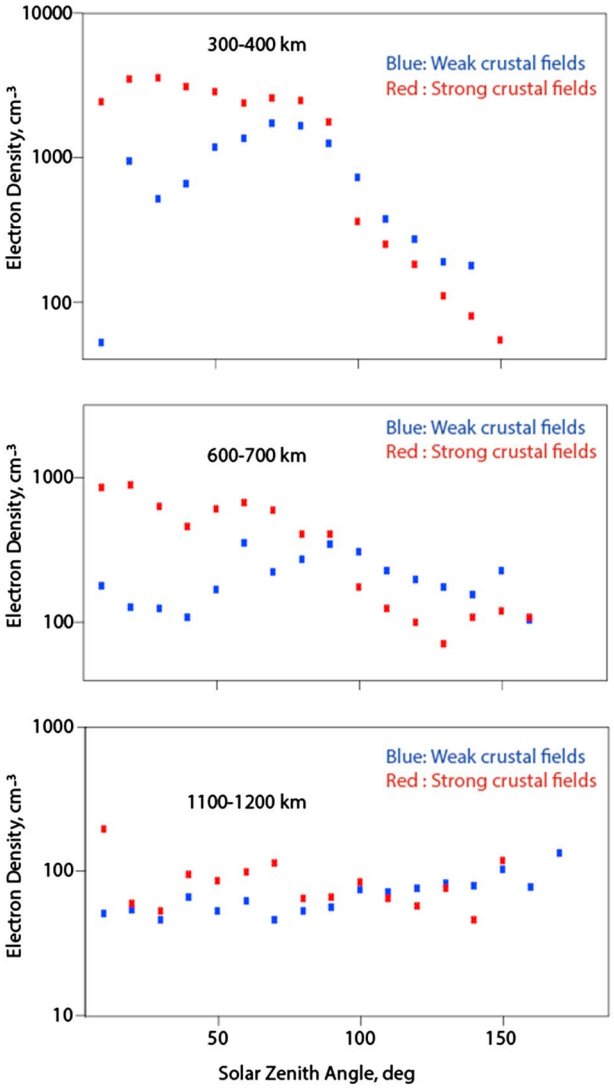

Figure 9. Median electron density as a function of SZA for the data from the region with latitude above 0° and all longitudes (blue dots), latitude below 0°, and longitudes between 150° and 240° (red dots) for 300–400 km (top panel), 600–700 km (middle panel), and 1,100–1,200 km (bottom panel).

9. Dependence on Crustal Fields

Mars does not have a global magnetic field, but has local, crustal, smaller-scale magnetic fields (Acuna et al., 1998; Cain et al., 2003), which affect many processes on Mars, including the ionospheric plasma boundaries and electron densities. Vertical crustal fields are known to cause bulges on the ionosphere (Duru et al., 2006). Brain et al. (2005) and Edberg et al. (2008) showed that the magnetic pile-up boundary is higher in strong crustal field regions. Andrews et al. (2014) used MARSIS data and concluded that dayside plasma densities have higher average values above strong crustal magnetic field regions. Recently, MAVEN observations showed that at altitudes above 200 km, the electron temperature is cooler and the electron densities are about 30% higher above regions with high crustal magnetic fields (Flynn et al., 2017). According to Monte Carlo simulations done by Jolitz et al. (2017) the presence of crustal fields reduces total ionization but increases the area of ionization. Fang et al. (2017) performed magnetohydrodynamic simulations, which showed that boundaries are affected by the global crustal fields.

Figure 9 displays median electron density as a function of SZA for fixed altitude ranges for two different regions on Mars: the northern hemisphere (blue dots), where the crustal fields are weak or nonexistent; and latitudes lower than 0° and longitudes between 150° and 240° (red dots), where the crustal fields are very strong. The top panel is for altitudes between 300 and 400 km, the middle panel is for 600–700 km, and the bottom panel is for between 1,100 and 1,200 km. There is a very clear dependence of the median electron density on the crustal magnetic fields; On the dayside, the median electron density is higher above the strong crustal field region. This is valid up to about 1,200 km, after which the effect cannot be observed anymore. The crustal fields are shown to be providing a shielding effect from the solar wind interaction and decrease the ion escape rates (Dong et al., 2015; Nagy et al., 2004). Also, multispecies single-fluid magnetohydrodynamic model results performed by Ma et al. (2014) show that the heavy ion densities are enhanced in the regions of high crustal fields, which supports our results.

On the nightside, the weak field region has higher electron densities at lower altitudes. However, since the electron densities are lower in general, the difference is not as prominent as on the dayside. Previous studies showed that nightside electron densities are lower at low altitudes (below 180 km; Girazian et al., 2017). This is because strong crustal fields act as a shield and reduce electron precipitation rates so that ions recombine without being replenished (Brain et al., 2007; Mitchell et al., 2001).

10. Conclusions

Thanks to MEX's 13 years of operation, we have more than 11 years of data, which gives us the possibility of making an extensive investigation on the electron densities on the Martian ionosphere, with an emphasis on the solar cycle, seasonal, and crustal field dependence.

The ionosphere of Mars is very dynamic, with electron density values changing in response to many parameters (Mendillo et al., 2017). The electron density shows variability from orbit to orbit and also within an orbit.

The observed SZA dependence of the electron density is compatible with previous studies and models. The median electron density is almost constant on the dayside. It decreases sharply past the terminator at low altitudes. At altitude above about 800 km, there is no difference between dayside and nightside.

The median electron density increases with decreasing altitude. The dependence is exponential with an *e*-folding height between 45 and 214 km between the subsolar point and 120°, corresponding to temperatures between 165 and 780 K. It is on the order of thousands up to 150° of SZA, after which the exponential increase is not observed. A model of the high-altitude plasma-scale height derived from the electron density profiles of Figure 5 gives a result of an exponential function. Both dayside- and nightside-scale heights increase with SZA, but the nightside scale height increases much more sharply with increasing SZA than that of the dayside. Presumably cross-longitude plasma transport allows plasma generated by photoionization to populate high altitudes.

The primary source of the dayside Martian ionosphere is the photoionization of the neutral atmosphere by solar radiation. Increased solar irradiation means increased EUV flux, which in turn leads to higher rates of photoionization. As a result, the median electron density depends on the solar activity. It is higher on average at solar maximum. During the northern hemisphere's summer the electron density is lower than the northern hemisphere's winter.

Finally, the dayside median electron density is considerably higher over strong crustal field regions than it is over weak field regions. The opposite is true on the nightside; the median plasma density is less in the high crustal magnetic field regions than elsewhere. The reason for this divergence appears to be inhibition of diffusion of ions by the strong magnetic fields. On the dayside, ions that are newly formed by photoionization are inhibited from diffusing out of the strong field regions, causing higher densities than in adjacent regions of weaker magnetic field. On the nightside, ion densities are depleted by recombination in the regions of strong field. These recombined ions cannot be replaced through diffusion because of the strong magnetic fields.

Acknowledgments
TIMED-SEE data from University of Colorado (http://lasp.colorado.edu/lisird/index.html). Work at Iowa was supported by NASA through contract 1224107 from the Jet Propulsion Laboratory. MARSIS data are available through the Planetary Data System at http://pdsgeosciences.wustl.edu. Authors would like to thank the referee for his valuable comments and corrections.

References

Acuna, M., Connerney, J. E. P., Wasilewski, P., Lin, R. P., Anderson, K. A., Carlson, C. W., et al. (1998). Magnetic field and plasma observations at Mars: Initial results of the Mars Global Surveyor mission. *Science*, *279*(5357), 1676–1680.

Andrews, D. J., Edberg, N. J. T., Eriksson, A. I., Gurnett, D. A., Morgan, D., Nemec, F., & Opgenoorth, H. J. (2014). Control of the topside Martian ionosphere by the crustal magnetic fields. *Journal of Geophysical Research: Sapce Physics*, *120*, 3042–3058. https://doi.org/10.1002/2014JA020703

Bougher, S. W., Jakosky, B., Halekas, J., Grebowsky, J., Luhmann, J., Mahaffy, P., et al. (2015). Early MAVEN deep dip campaign reveals thermosphere and ionosphere variability. *Science*, *350*, 6261. https://doi.org/10.1126/science.aas0459

Bougher, S. W., Pawlowski, D., Bell, J. M., Nelli, S., McDunn, T., Murphy, J. R., et al. (2015). Mars global ionosphere-thermosphere model: Solar cycle, seasonal, and diurnal variations of the Mars upper atmosphere. *Journal of Geophysical Research: Planets*, *120*, 311–342. https://doi.org/10.1002/2014JE004715

Brain, D. A., Halekas, J. S., Lillis, R., Mitchell, D. L., Lin, R. P., & Crider, D. H. (2005). Variability of the altitude of the Martian sheath. *Geophysical Research Letters*, *32*, L18203. https://doi.org/10.1029/2005GL023126

Brain, D. A., Lillis, R. J., Mitchell, D. L., Halekas, J. S., & Lin, R. P. (2007). Electron pitch angle distributions as indicators of magnetic field topology near Mars. *Journal of Geophysical Research*, *112*, A09201. https://doi.org/10.1029/2007JA012435

Cain, J. C., Ferguson, B. B., & Mozzoni, D. (2003). An $n = 90$ internal potential function of the Martian crustal magnetic field. *Journal of Geophysical Research*, *108*(E2), 5008. https://doi.org/10.1029/2000JE001487

Chicarro, A., Martin, P., & Traunter, R. (2004). Mars Express: A European mission to the red planet. In A. Wilson (Ed.), *Mars Express, the scientific payload, SP-1240*, (pp. 3–16). Noordwijk, Netherlands: ESA Publication Division.

Dong, C., Bougher, S. W., Ma, Y., Toth, G., Lee, Y., Nagy, A. F., et al. (2015). Solar wind interaction with Martian upper atmosphere: Crustal field orientation, solar cycle and seasonal variations. *Journal of Geophysics Research: Space Physics*, *120*, 7857–7872. https://doi.org/10.1002/2015JA020990

Duru, F., Gurnett, D. A., Averkamp, T. F., Kirchner, D. L., Huff, R. L., Persoon, A. M., et al. (2006). Magnetically controlled structures in the ionosphere of Mars. *Journal of Geophysical Research*, *111*, A12204. https://doi.org/10.1029/2006JA011975

Duru, F., Gurnett, D. A., Morgan, D. D., Modolo, R., Nagy, A. F., & Najib, D. (2008). Electron densities in the upper ionosphere of Mars from the excitation of electron plasma oscillations. *Journal of Geophysical Research*, *113*, A07302. https://doi.org/10.1029/2008JA013073

Duru, F., Gurnett, D. A., Morgan, D. D., Winningham, J. D., Frahm, R. A., & Nagy, A. F. (2011). Nightside ionosphere of Mars studied with local electron densities: A general overview and electron density depressions. *Journal of Geophysical Research*, *116*, A10316. https://doi.org/10.1029/2011JA016835

Duru, F., Gurnett, D. A., Winningham, J. D., Frahm, R., & Modolo, R. (2010). A plasma flow velocity boundary at Mars from the disappearance of electron plasma oscillations. *Icarus*, *206*(1), 74–82. https://doi.org/10.1016/j.icarus.2009.04.012

Edberg, N. J. T., Lester, M., Cowley, S. W. H., & Eriksson, A. I. (2008). Statistical analysis of the location of the Martian magnetic pileup boundary and bow shock and the influence of crustal magnetic fields. *Journal of Geophysical Research*, *113*, A08206. https://doi.org/10.1029/2008JA013096

Ergun, R. E., Morooka, M. W., Andersson, L. A., Fowler, C. M., Delory, G. T., Andrews, D. J., et al. (2015). Dayside electron temperature and density profiles at Mars: First results from the MAVEN Langmuir probe and waves instrument. *Geophysical Research Letters*, *42*, 8846–8853. https://doi.org/10.1002/2015GL065280

Fang, X., Ma, Y., Masunaga, K., Dong, Y., Brain, D., Halekas, J., et al. (2017). The Mars crustal magnetic field control of plasma boundary locations and atmospheric loss: MHD prediction and comparison with MAVEN. *Journal of Geophysical: Research*, *122*, 4117–4137. https://doi.org/10.1002/2016JA023509

Fjeldbo, G., Fjeldbo, W. C., & Eshleman, V. R. (1966). Models for the atmosphere of Mars based on the Mariner 4 occultation experiment. *Journal of Geophysical Research*, *71*(9), 2307–2316. https://doi.org/10.1029/JZ071i009p02307

Flynn, C. L., Vogt, M. F., Withers, P., Andersson, L., England, S., & Liu, G. (2017). MAVEN observations of the effect of crustal magnetic fields on the electron density and temperature in the Martian dayside ionosphere. *Geophysical Research Letters*, *44*, 10,812–10,821. https://doi.org/10.1002/2017GL075367

Fowler, C. M., Andersson, L., Ergun, R. E., Morooka, M., Delory, G., Andrews, D. J., et al. (2015). The first in situ electron temperature and density measurements of the Martian nightside ionosphere. *Geophysical Research Letters*, *42*, 8854–8861. https://doi.org/10.1002/2015GL065267

Fox, J. L., Yeager, K. E. & (2009). MGS electron density profiles: Analysis of the peak magnitudes. *Icarus*, *200*, 468–479.

Girazian, Z., Mahaffy, P., Lillis, R. J., Benna, M., Elrod, M., Fowler, C. M., & Mitchell, D. L. (2017). Ion densities in the nightside ionosphere of Mars: Electron impact ionization. *Geophysical Research Letters*, *44*, 11,248–11,256. https://doi.org/10.1002/2017GL075431

Gurnett, D. A., & Bhattacharjee, A. (2005). *Introduction to plasma physics with space and laboratory applications*. Cambridge: Cambridge University Press. https://doi.org/10.1017/CBO9780511809125

Gurnett, D. A., Kirchner, D. L., Huff, R. L., Morgan, D. D., Persoon, A. M., Averkamp, T. F., et al. (2005). Radar soundings of the ionosphere of Mars. *Science*, *310*(5756), 1929–1933. https://doi.org/10.1126/science.1121868

Gurnett, D. A., Morgan, D. D., Duru, F., Akalin, F., Winningham, J. D., Frahm, R. A., et al. (2010). Large density fluctuations in the Martian ionosphere as observed by the Mars express radar sounder. *Icarus*, *206*(1), 83–94. https://doi.org/10.1016/j.icarus.2009.02.019

Halekas, J. S., Ruhunusiri, S., Harada, Y., Collinson, G., Mitchell, D. L., Mazelle, C., et al. (2017). Structure, dynamics, and seasonal variability of the Mars-solar wind interaction: MAVEN Solar Wind Ion Analyzer in-flight performance and science results. *Journal of Geophysical Research: Space Physics*, *122*, 547–578. https://doi.org/10.1002/2016JA023167

Hanson, W. B., Sanatani, S., & Zuccaro, D. R. (1977). The Martian ionosphere as observed by the Viking retarding potential analyzers. *Journal of Geophysical Research*, *82*(28), 4351–4363. https://doi.org/10.1029/JS082i028p04351

Jakosky, B., Lin, R. P., Grebowsky, J. M., Luhmann, J. G., Mitchell, D. F., Beutelschies, G., et al. (2015). The Mars Atmosphere and Volatile EvolutioN (MAVEN) mission. *Space Science Reviews*, *195*(1-4), 3–48. https://doi.org/10.1007/s11214-015-0139-x

Jolitz, R. D., Dong, C. F., Lee, C. O., Lillis, R. J., Brain, D. A., Curry, S. M., et al. (2017). A Monte Carlo model of crustal field influences on solar energetic particle precipitation into the Martian atmosphere. *Journal of Geophysical Research: Space Physics*, *122*, 5653–5669. https://doi.org/1002/2016JA023781

Kliore, A., Cain, D. L., Levy, G. S., Eshleman, V. R., Fjeldbo, G., & Drake, F. D. (1965). Occultation experiment: Results of the first direct measurement of Mars's atmosphere and ionosphere. *Science*, *149*(3689), 1243–1248. https://doi.org/10.1126/science.149.3689.1243

Lundin, R., Barabash, S., Holmstrom, M., Nilsson, H., Futaana, Y., Ramstad, R., et al. (2013). Solar cycle effects on the ion escape from Mars. *Geophysical Research Letters*, *40*, 6028–6032. https://doi.org/10.1002/2013GL058154

Ma, Y., Fang, X., Russell, C. T., Nagy, A. F., Toth, G., Luhmann, J. G., et al. (2014). Effects of crustal field rotation on the solar wind plasma interaction with Mars. *Geophysical Research Letters*, *41*, 6563–6569. https://doi.org/10.1002/2014GL060785

Mahaffy, P. R., Benna, M., Elrod, M., Yelle, R. V., Bougher, S. W., Stone, S. W., & Jakosky, B. M. (2015). Structure and composition of the neutral upper atmosphere of Mars from the MAVEN NGIMS investigation. *Geophysical Research Letters*, *42*, 8951–8957. https://doi.org/10.1002/2015GL065329

Mendillo, M., Narvaez, C., Vogt, M. F., Mayyasi, M., Forbes, J., Galand, M., et al. (2017). Sources of ionospheric variability at Mars. *Journal of Geophysical Research: Space Physics*, *122*, 9670–9684. https://doi.org/10.1002/2017JA024366

Mitchell, D. L., Lin, R. P., Mazelle, C., Rème, H., Cloutier, P. A., Connerney, J. E. P., et al. (2001). Probing Mars' crustal magnetic field and ionosphere with the MGS electron reflectometer. *Journal of Geophysical Research*, *106*(E10), 23,419–23,427. https://doi.org/doi:10.1029/2000JE001435

Morgan, D. D., Gurnett, D. A., Kirchner, D. L., Fox, J. L., Nielson, E., Plaut, J. J., & Picardi, G. (2008). Variations of Mars's ionospheric electron density from Mars Express radar soundings. *Journal of Geophysical Research*, *113*, A09303. https://doi.org/10.1029/2008JA013313

Nagy, A. F., Winterhalter, D., Sauer, K., Cravens, T. E., Brecht, S., Mazelle, C., et al. (2004). The plasma environment of Mars. *Space Science Reviews*, *111*(1/2), 33–114. https://doi.org/10.1023/B:SPAC.0000032718.47512.92

Patzold, M., Tellmann, S., Hausler, B., Hinson, D., Schaa, R., & Tyler, G. L. (2005). A sporadic third layer in the ionosphere of Mars. *Science*, *310*(5749), 837–839. https://doi.org/10.1126/science.1117755

Picardi, G., Biccari, D., Seu, R., Plaut, J., Johnson, W. T. K., Jordan, R. L., et al. (2004). MARSIS: Advanced radar for subsurface and ionosphere sounding. In *Mars Express: A European mission to the Red Planet, SP-1240*, (pp. 51–70). Noordwijk, Netherlands: ESA Publ. Division.

Rahmati, A., Larson, D. E., Cravens, T. E., Lillis, R. J., Halekas, J. S., McFadden, J. P., et al. (2018). Seasonal variability of neutral escape from Mars as derived from MAVEN pickup ion observations. *Journal of Geophysical Research: Planets*, *123*, 1192–1202. https://doi.org/10.1029/2018JE005560

Sanchez-Cano, B., Lester, M., Witasse, O., Milan, S. E., Hall, B. E. S., Cartacci, M., et al. (2016). Solar cycle variations in the ionosphere of Mars as seen by multiple Mars Express data sets. *Journal of Geophysical Research: Space Physics*, *121*, 2547–2568. https://doi.org/10.1002/2015JA022281

Schunk, R. W., & Nagy, A. F. (2009). *Ionospheres: Physics, plasma physics, and chemistry*, *Cambridge Atmospheric and Space Science Series*, (2nd ed.). Cambridge: Cambridge University Press. https://doi.org/10.1017/CBO9780511635342

Valeille, A., Combi, M. R., Bougher, S. W., Tenishev, V., & Nagy, A. F. (2009). Three-dimensional study of Mars upper thermosphere/ionosphere and hot oxygen corona: 2. Solar cycle, seasonal variations, and evolution over history. *Journal of Geophysical Research*, *114*, E11006. https://doi.org/10.1029/2009JE003389

Vignes, D., Mazelle, C., Reme, H., Acunã, M. H., Connerney, J. E. P., Lin, R. P., et al. (2000). The solar wind interaction with Mars: Locations and shapes of the bow shock and magnetic pile-up boundary from the observations of the MAG/ER experiment onboard Mars Global Surveyor. *Geophysical Research Letters*, *27*(1), 49–52. https://doi.org/10.1029/1999GL010703

Withers, P., & Mendillo, M. (2005). Response of peak electron densities in the martian ionosphere to day-to-day changes in solar flux due to solar rotation. *Planet Space Science*, *53*, 1401–1418.

Withers, P., Morgan, D. D., & Gurnett, D. A. (2014). Variations in peak electron densities in the ionosphere of Mars over a full solar cycle. *Icarus*, *251*, 5–11. https://doi.org/10.1016/j.icarus.2014.08.008

Yamauchi, M., Hara, T., Lundin, R., Dubinin, E., Fedorov, A., Sauvaud, J. -A., et al. (2015). Seasonal variations of Martian pick-up ions: Evidence of breathing exosphere. *Planetary and Space Science*, *119*, 54–61. https://doi.org/10.1016/j.pss.2015.09.013

Zhang, M. H. G., Luhmann, J. G., & Kliore, A. J. (1990). An observational study of the nightside ionospheres of Mars and Venus with radio occultation methods. *Journal of Geophysical Research*, *95*(A10), 17095. https://doi.org/10.1029/JA095iA10p17095